RSC Advances

PAPER

View Article Online
View Journal | View Issue

Cite this: *RSC Adv.*, 2015, **5**, 65635

Thermal property of an aggregation-induced emission fluorophore that forms metal–ligand complexes with $Zn(ClO_4)_2$ of salicylaldehyde azine-functionalized polybenzoxazine†

Mohamed Gamal Mohamed,[a] Ruey-Chorng Lin,[a] Jia-Huei Tu,[a] Fang-Hsien Lu,[a] Jin-Long Hong,[a] Kwang-Un Jeong,[c] Chih-Feng Wang[d] and Shiao-Wei Kuo*[ab]

In this report, we designed a new and simple salicylaldehyde azine-functionalized benzoxazine (azine-BZ) monomer *via* Mannich condensation reaction of aniline and paraformaldehyde with 1,2-bis(2,4-dihydroxybenzylidene)hydrazine in 1,4-dioxane. Compared with 3-phenyl-3,4-dihydro-2*H*-benzoxazine monomer (263 °C), the maximum exothermic peak of azine-BZ shifted to a lower temperature (213 °C) based on differential scanning calorimetry (DSC) analyses because of the basicity of the phenolic group (OH) in the *ortho* position and the azine groups. Blending azine-BZ with different weight ratios of zinc perchlorate [$Zn(ClO_4)_2$] to form benzoxazine/zinc ion complexes not only affected the thermal properties based on thermogravimetric analysis (TGA) due to physical crosslinking through metal–ligand interactions but also expedited the ring-opening polymerization, decreasing the curing temperature from 213 to 184 °C (at 10 wt% Zn^{2+}). Based on the fluorescence results, the azine-BZ and azine-BZ/$Zn(ClO_4)_2$ complexes were non-emissive in a THF solution. Their fluorescence increased gradually upon the addition of water. Interestingly, both the pure azine-BZ and $Zn(ClO_4)_2$-blended complex still emitted light after thermal curing at 150 °C, as determined through photoluminescence measurements, indicating that the azine group could act as a probe of the curing behavior of the benzoxazine monomer, as well as a fluorescent chemosensor for Zn^{2+} and, possibly, other transition metal ions through a metal–ligand charge transfer mechanism.

Received 19th May 2015
Accepted 14th July 2015

DOI: 10.1039/c5ra09409g

www.rsc.org/advances

Introduction

Benzoxazine monomer is a molecule containing an oxazine ring (a heterocyclic six-membered ring with oxygen and nitrogen atoms) connected to a benzene ring. In the last few decades, polybenzoxazines (PBZs), a class of thermosetting resins, have been studied widely due to their specific potential applications as phenolic resin materials.[1–3] Polybenzoxazines (PBZs) are produced by the thermal curing of oxazine ring in benzoxazine monomer without any catalyst, affording a highly dense cross-linked network material with strong intra- and inter-molecular hydrogen bonding between phenolic groups and tertiary amine in the Mannich linkage after ring-opening polymerization.[4] Numerous literatures report the potential applications of polybenzoxazines in industrial fields due to their unique characteristics such as flame resistance, low surface energies, high thermal and mechanical stabilities, and low water adsorption.[5,6]

BZs are versatile thermoset resins that are synthesized through Mannich condensation between an aromatic phenol, a primary amine, and formaldehyde.[7–12] Nowadays, these phenolic resins can be used as thermosets to prepare polymer nanocomposites due to their unique and excellent thermal properties.[13–16] Polybenzoxazine chemistry offers flexibility of numerous molecular designs, thereby facilitating the preparation of different PBZ nanocomposites. To control the properties of PBZs, several derivatives functionalized with reactive groups (*e.g.*, propargyl, nitrile, alkyl, carboxyl, and hydroxyalkyl) have been synthesized.[17–20] Two types of BZ-based composites have been developed: fiber-reinforced PBZ composites and inorganic particle-reinforced PBZ composites (*e.g.*, silica, TiO_2, and magnetic nanoparticles).[21]

Most fluorescent materials weaken the emissive properties when they aggregate in a poor solvent or in the solid state. This

[a]*Department of Materials and Optoelectronic Science, Center for Functional Polymers and Supramolecular Materials, National Sun Yat-Sen University, Kaohsiung, Taiwan. E-mail: kuosw@faculty.nsysu.edu.tw*

[b]*Department of Medicinal and Applied Chemistry, Kaohsiung Medical University, Kaohsiung, Taiwan*

[c]*Department of Polymer-Nano Science and Technology, Chonbuk National University, Jeonju, Korea*

[d]*Department of Materials Science and Engineering, I-Shou University, Kaohsiung, Taiwan*

† Electronic supplementary information (ESI) available: FTIR, UV, MS, and ^1H NMR spectra of pure azine-BZ. See DOI: 10.1039/c5ra09409g

phenomenon, known as aggregation-caused quenching (ACQ),[22,23] greatly decreases the applicability of such materials as organic light-emitting materials or fluorescent chemosensors.[24–26] At the beginning of this century, Tang *et al.* reported that numerous materials can emit light when dispersed in a poor solvent or fabricated into film in a nano-aggregate state. These interesting phenomena are named aggregation-induced emission (AIE) or aggregation-induced enhanced emission (AIEE).[27,28] AIE fluorescent materials become very strongly emissive in the aggregate or solid states, but become very strong emitters when aggregated as powders or nano-aggregates. There are numerous mechanisms behind AIE, including restricted intramolecular rotation (RIR),[29,30] twisting intramolecular charge transfer (TICT)[31] and planarity and rotation ability.[32] Tang *et al.* also reported that a series of salicylaldehyde azine derivatives exhibited AIE characteristics in good solvents, but displayed very weak emissions while being strongly luminescent in poor solvents.[33] Several fluorescent chemosensors reported have been designed based on the mechanisms of photoinduced electron transfer (PET),[34] fluorescence resonance intramolecular charge transfer (FRICT),[35] and metal–ligand charge transfer (MLCT).[36] Tang *et al.* reported that Schiff base-modified triphenylaminobenzimidazole and pyridinecarboxaldehyde derivatives displaying AIEE characteristics acted as chemosensors for Cu(II) and Zn(II) ions.[37]

Therefore, in this article, we synthesized a new BZ monomer containing a salicylaldehyde azine unit (azine-BZ) through facile and simple Mannich condensation reaction of 1,2-bis(2,4-dihydroxybenzylidene)hydrazine (CN_4OH), paraformaldehyde, and aniline in the presence of 1,4-dioxane as a good solvent (Scheme 1). We also studied the thermal curing polymerization, thermal stabilities, absorption and emission behavior, and specific metal–ligand interaction when azine-BZ was blended with various weight ratios of zinc perchlorate [$Zn(ClO_4)_2$] before and after thermal curing *via* chelation complexes using differential scanning calorimetry (DSC), Fourier transform infrared (FTIR) spectroscopy, thermogravimetric analysis (TGA), UV-Vis and photoluminescence (PL) spectroscopy. In addition, we used transmission electron microscopy (TEM) and dynamic light scattering (DLS) to characterize the self-assembled nano-aggregates morphology, which formed from the azine-BZ monomer in THF/water solvent pairs.

Experimental section

Materials

Paraformaldehyde (96%), aniline, and 2,4-dihydroxybenzaldehyde were used as received from Acros. Ethyl acetate (EA), hydrazine monohydrate (98%), chloroform, dichloromethane, ethanol, tetrahydrofuran (THF), and 1,4-dioxane were used as received from Scharlau. Zinc perchlorate hexahydrate [$Zn(ClO_4)_2 \cdot 6H_2O$] was purchased from Aldrich and dried overnight in a vacuum oven at 70 °C to remove water.

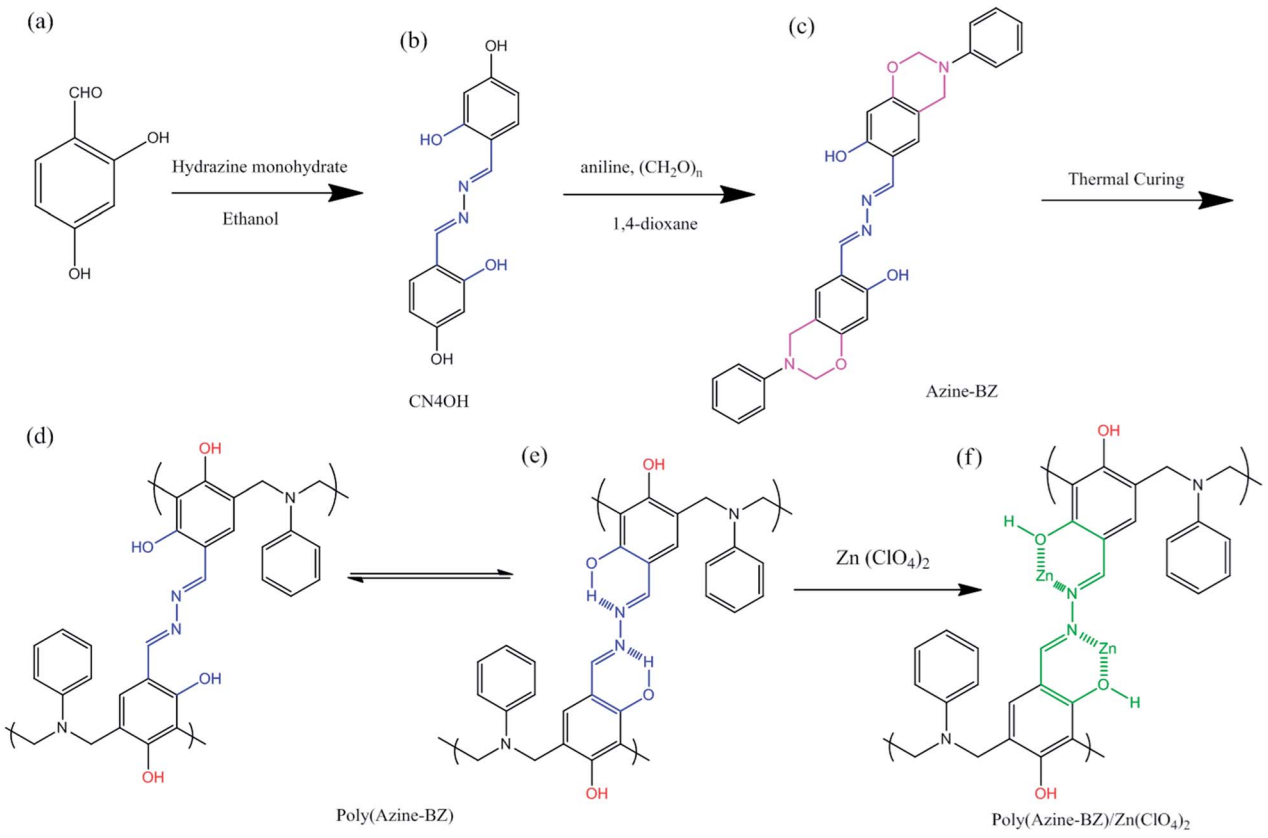

Scheme 1 Synthesis and chemical structures of (a) 2,4-dihydroxybenzaldehyde, (b) CN_4OH, (c) azine-BZ, (d and e) poly(azine-BZ), and (f) the poly(azine-BZ)/$Zn(ClO_4)_2$ complex.

bis(2,4-Dihydroxybenzylidene)hydrazine (CN_4OH)[33,38]

Under a N_2 atmosphere in a 150 mL two-neck round-bottom flask equipped with a stirrer bar, hydrazine monohydrate (0.900 g, 18.1 mmol) and 2,4-dihydroxybenzaldehyde (5.00 g, 36.2 mmol) were dissolved in absolute EtOH (100 mL). After stirring overnight at room temperature, the precipitate was filtered and washed three times with EtOH. The yellow powder was recrystallized from a small amount of THF, affording yellow crystals (8.50 g, 86%); FTIR (KBr, cm^{-1}): 3200–3400 (OH stretching). ^1H NMR (500 MHz, DMSO-d_6, δ, ppm): 11.94 (s, 1H, OH_a), 10.10 (s, 1H, OH_b), 8.75 (d, 2H, H_c), 7.36 (t, 2H, H_d), 7.04 (d, 1H, H_e), 6.96 (t, 1H, H_f). ^{13}C NMR (125 MHz, DMSO-d_6, δ, ppm): 162.9, 162.6, 161.5, 133.6, 110.8, 110.8, 108.8, 103.1. High resolution FT-MS (m/z) for MH^+ ($C_{14}H_{12}N_2O_4$): 273.09: calc.: 272.08 (Fig. S2†).

Synthesis of azine-BZ[39]

50 mL of 1,4-dioxane/ethanol, paraformaldehyde (0.882 g, 29.4 mmol), 1,2-bis(2,4-dihydroxybenzylidene)hydrazine [(CN_4OH), (2.00 g, 7.35 mmol)], and aniline (1.37 g, 14.7 mmol) were mixed in a 150 mL two-neck round-bottom flask under a N_2 atmosphere with a reflux condenser. The reaction solution was heated under reflux for 18 h at 90–110 °C. After cooling the reaction mixture to room temperature, the solvent was evaporated under reduced pressure to give a yellow solid, which was purified through column chromatography (SiO_2; EtOAc) to give a yellow solid (3.21 g, 87%). FTIR (KBr, cm^{-1}): 3300–3200 (OH stretching), 931 and 1488 (vibrations of trisubstituted benzene ring). ^1H NMR (500 MHz, $CDCl_3$, δ, ppm): 11.93 (s, 1H, H_a), 8.71 (s, 1H, H_b), 4.70 (s, 2H, Ar-CH_2–N), 5.33 (s, 2H, O–CH_2–N), 6.92–8.43 (m, CH aromatic). ^{13}C NMR (125 MHz, $CDCl_3$, δ, ppm): 45.93 (CCH_2N), 80.04 (OCH_2N). High resolution FT-MS (m/z) for MH^+ ($C_{14}H_{12}N_2O_4$): 507.20: calc.: 506.20 (Fig. S3†).

Poly(azine-BZ)/zinc complexes

$Zn(ClO_4)_2$ (1, 2, 3, 4, 5, or 10 wt%) was dissolved in 5 mL of THF for 1 h. Then, $Zn(ClO_4)_2$ solutions were added dropwise to azine-Bz solutions. Furthermore, the azine-Bz/$Zn(ClO_4)_2$ complex solutions were stirred for 2 days, and the solvent was removed under reduced pressure. Each blended mixture was poured into a stainless-steel mold and polymerized in a stepwise manner, with heating at 110, 150, 180, 210, and 240 °C for 2 h at each temperature. The color of each cured sample was dark red.

Nanoaggregates of azine-BZ and azine-BZ/zinc complexes

Stock solutions of azine-BZ and azine-BZ/Zinc were prepared in THF in a 100 mL volumetric flask with concentrations of 1×10^{-4} M. Then, water (poor solvent) was added dropwise under vigorous stirring to prepare different volume ratios (0–90%). PL spectra of the suspension of nano-aggregates were obtained immediately.

Characterization

Nuclear magnetic resonance (^1H and ^{13}C NMR) spectra were obtained on an INOVA 500 using DMSO-d_6 and $CDCl_3$ as solvents. Fourier transform infrared (FTIR) spectra of the KBr disks of CN_4OH and azine-BZ were acquired by a Bruker Tensor 27 FTIR spectrophotometer and thirty-two scans were collected at a spectral resolution of 4 cm^{-1}. Differential scanning calorimetry (DSC) measurements were conducted with a TA Q-20 operated under N_2 as the purge gas (50 mL min^{-1}) at a heating rate of 20 °C min^{-1}. The sample (*ca.* 3–5 mg) was placed in a sealed aluminum sample pan. Dynamic curing scans were recorded from 30 to 350 °C at a heating rate of 20 °C min^{-1}. The thermal stabilities of the samples were measured using a TA Q-50 thermogravimetric analyzer operated under N_2 as the purge gas (60 mL min^{-1}) at heating rate of 20 °C min^{-1} from 30 to 800 °C. UV-Vis spectra were obtained using a Shimadzu mini 1240 spectrophotometer; the concentration of azine-BZ in THF was 10^{-4} M. Photoluminescence spectra was collected at room temperature using a monochromatized Xe light source. Particle sizes of the aggregates in solution were measured by DLS using a Brookhaven 90 plus spectrometer equipped with a temperature controller. An argon laser operating at 658 nm was used as the light source. TEM images were recorded using a JEOL-2100 transmission electron microscope

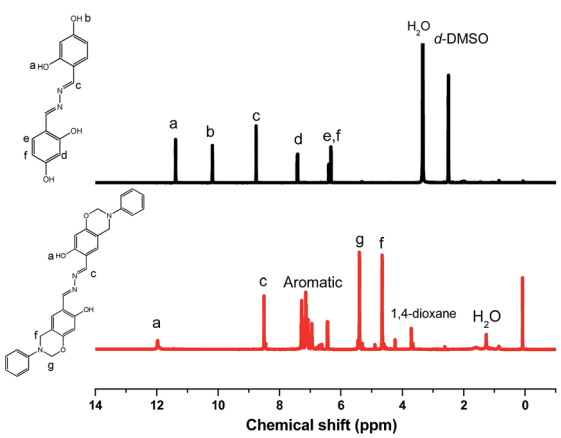

Fig. 1 ^1H NMR spectra of (a) CN_4OH and (b) azine-BZ.

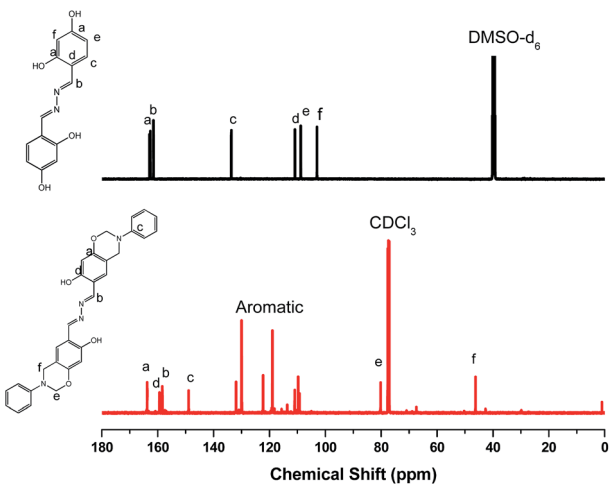

Fig. 2 ^{13}C NMR spectra of (a) CN_4OH and (b) azine-BZ.

operated at an accelerating voltage of 200 kV. The molecular weights of CN_4OH and azine-BZ were recorded using a Bruker Solarix high resolution Fourier Transform Mass spectroscopy system FT-MS (Bruker, Bremen, Germany).

Results and discussion

Synthesis and characterization of CN_4OH and azine-BZ

Scheme 1 displays our synthesis of the salicylaldehyde azine-functionalized BZ monomer (azine-BZ). First, we carried out a Schiff base condensation of 2,4-dihydroxybenzaldehyde with hydrazine monohydrate in EtOH to obtain CN_4OH. Then, we prepared azine-BZ with high purity (more than 95%) through a Mannich condensation reaction of CN_4OH, paraformaldehyde, and aniline in 1,4-dioxane at 80–90 °C. We carefully confirmed the chemical structures of CN_4OH and azine-BZ *via* ^1H NMR, ^{13}C NMR, and FTIR spectroscopy. Fig. 1 illustrates the ^1H NMR spectra of CN_4OH and azine-BZ. The spectrum of CN_4OH [Fig. 1(a)] features signals at 10.10 and 11.94 ppm, representing the OH groups of the phenolic units, as well as signals in the range 6.33–7.40 ppm for the aromatic protons and at 8.69 ppm for the N=CH groups. The spectrum of the AIE unit (azine)-based BZ monomer [Fig. 1(b)] lacked the peak at 10.10 ppm for the OH_b proton of CN_4OH, but featured peaks at 6.36–7.26 ppm for the aromatic protons and resonances at 4.70 ($ArCH_2N$) and 5.33 (OCH_2N) ppm at a 1 : 1 ratio; moreover, no signal was present near 4.0 ppm, corresponding to an NCH_2Ph unit, as a result of ring opening of the BZ moiety. No other major peaks were evident in the ^1H NMR spectra, indicating that azine-BZ had successfully formed. Fig. 2 presents the ^{13}C NMR spectra of CN_4OH and azine-BZ. The spectrum of CN_4OH [Fig. 2(a)] features signals for the carbon nuclei in the aromatic rings and double bonds in the range 103.77–163.27 ppm. The spectrum of azine-BZ [Fig. 2(b)] displays characteristic resonances for the $ArCH_2N$ and OCH_2N units of the oxazine ring at 45.93 and 80.05 ppm, respectively. Fig. S1† presents the FTIR spectra of CN_4OH and azine-BZ, obtained at room temperature. The spectrum of CN_4OH [Fig. S1(a)†] features three sharp peaks at 3217, 3481, and 3522 cm^{-1} for the intra- and inter-molecular hydrogen-bonded and free OH groups, and sharp signals for the aromatic rings at 831, 1599, 1619, and 3033 cm^{-1}. The spectrum of azine-BZ [Fig. S1(b)†] features characteristic absorption bands at 1366 cm^{-1} (tetrasubstituted benzene ring), 1225 cm^{-1} (asymmetric COC stretching), 1042 cm^{-1} (symmetric COC stretching), and 931 cm^{-1} (stretching vibrations of oxazine ring).

High resolution FT-MS displayed the exact molecular weights of CN_4OH and azine-BZ (ESI Fig. S2 and S3†). These spectral data are consistent with the successful synthesis of a new azine-BZ monomer.

Optical properties and AIE of CN_4OH and azine-BZ

The UV-Vis absorption spectrum of azine-BZ monomer in THF (1×10^{-4} M) features (Fig. S4†) an absorption peak at 370 nm,

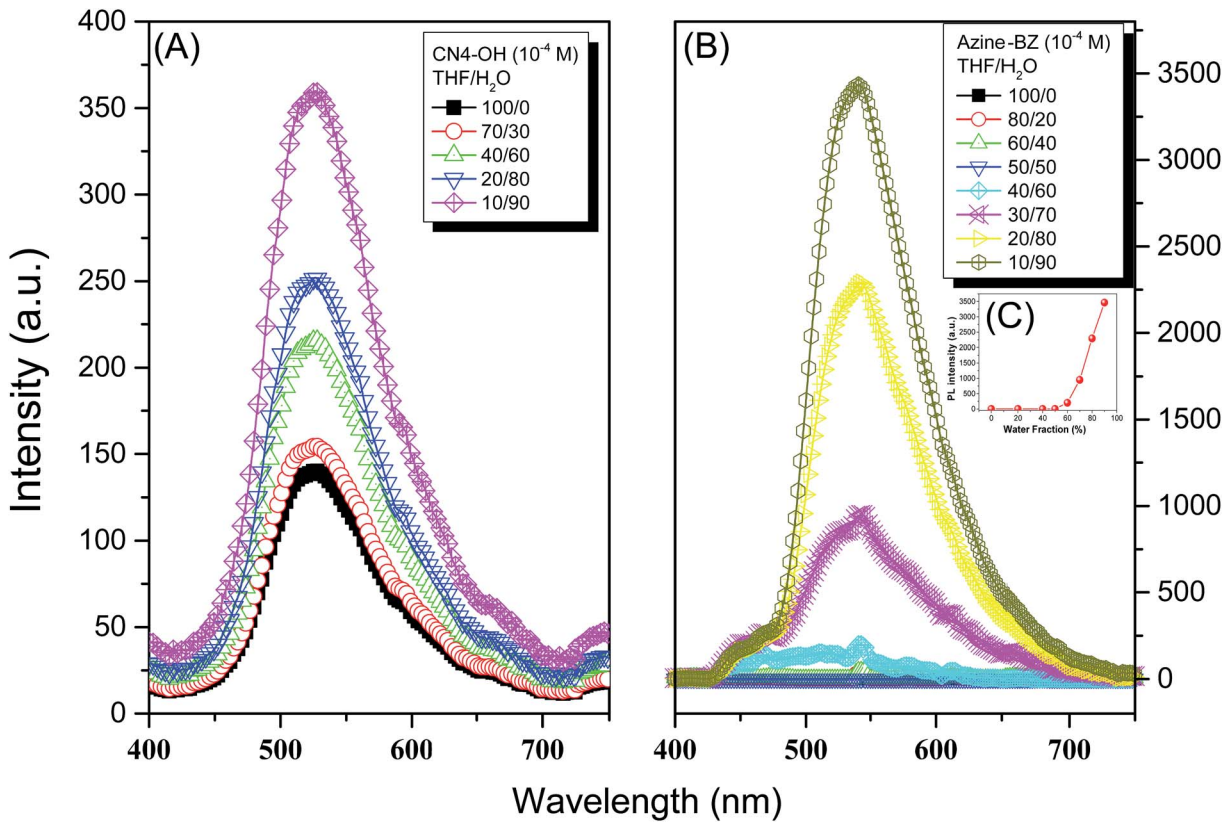

Fig. 3 PL spectral changes of (A) CN_4OH and (B) azine-BZ (1.0×10^{-4} mol L^{-1}) and (C) PL intensity of azine-BZ in THF/water mixtures at various water fractions.

which can be attributed to the π–π* transition of the salicylaldehyde azine unit. Most reported salicylaldehyde azines are fluorescent AIE materials that can emit different light in their aggregated states, presumably because of RIR and excited state intramolecular proton transfer [ESIPT].[33,38] We investigated the AIE phenomena of CN_4OH and azine-BZ in THF/H_2O mixtures at water contents in the range of 0–90%. CN_4OH and azine-BZ are both soluble in common organic solvents (THF, DMSO, DMF), but insoluble in water and hexane. As expected, solutions of CN_4OH and azine-BZ in THF are virtually non-luminescent, as determined from their fluorescence spectra [Fig. 3(A) and (B)]. However, the fluorescence intensities increased gradually when the water content was greater than 80% for CN_4OH and 90% for azine-BZ [Fig. 3(C)], with the emissions of CN_4OH and azine-BZ turning on and displaying green fluorescence. These emissions from CN_4OH and azine-BZ were presumably induced through aggregate formation, suggesting that both CN_4OH and azine-BZ exhibit AIE. In addition, we found that azine-BZ could form nanoparticles in a solution; moreover, we used transmission electron microscopy (TEM) and dynamic light scattering (DLS) to.investigate the growth of these nano-aggregates at high water contents of 90% (Fig. 4). The TEM images in Fig. 4(b) and (c) reveal nano-aggregates having sizes of approximately 100–200 nm, consistent with the DLS data. The particle sizes decreased upon increasing water content, reaching approximately 215 nm when the water content was 90 wt% [Fig. 4(a)]. The particle sizes determined from the TEM images were smaller than those measured using DLS because evaporation was necessary to prepare the samples for TEM, unavoidably leading to collapse and shrinkage of the particles. We suspect that CN_4OH and azine-BZ emitted intensely in their aggregated states because the large amount of water leads to the formation of spherical nano-aggregated structures thereby restricting intramolecular rotation of the phenyl ring rotors of CN_4OH and azine-BZ.

Thermal curing and AIE of azine-BZ

Differential scanning calorimetry (DSC) is a convenient and simple method to understand and investigate the study of the thermal curing and ring-opening polymerization of the azine-BZ monomer. The DSC thermograms of the pure azine-BZ monomer, recorded at a heating rate of 20 °C min^{-1} from 20 to 350 °C, reveal [Fig. 5(A)] an exothermic peak with the curing temperature at 213 °C and a reaction heat of 262 J g^{-1}. Based on the DSC profile, the polymerization exotherm maximum temperature for azine-BZ (213 °C) was lower than that (263 °C) for conventional 3-phenyl-3,4-dihydro-2*H*-benzoxazine (Pa-type),[1] presumably because the basic azine group in the backbone structure catalyzed the ring-opening polymerization. Clearly, after the thermal treatment of azine-BZ at 180 and 240 °C for 2 h at each temperature, the maximum exothermic peak completely disappeared, which indicates the completion of ring-opening polymerization of azine-BZ. We also studied the thermal polymerization of azine-BZ at elevated temperatures in Fig. 5(B). Fig. 5(B) displays that the intensities of the characteristic absorption bands of antisymmetric COC and out-of-plane benzene mode attached to benzene ring gradually disappear after thermal curing at 180 °C, corresponding to the ring-opening of benzoxazine monomer and formation of poly(azine-BZ). In addition, a new absorption signal appearing at 3433 cm^{-1} corresponds to the released OH group, consistent with the DSC analyses.

Thermal stability of azine-BZ after various thermal treatments has been investigated by thermogravimetric analysis, as shown in Fig. 6. Our TGA analysis revealed (Fig. 6) that the initial thermal decomposition temperature (T_{d5}) was strongly dependent on the curing exothermic peak in the DSC analysis [Fig. 5(A)]. For example, the initial thermal decomposition temperatures were near 215 and 233 °C when the curing temperatures were 110 and 150 °C, respectively; these values are close to the curing exothermic peaks in the DSC analyses in Fig. 5(A). In addition, the value of T_{d5} and the char yield both increased upon increasing the curing temperature. When the curing temperature was 240 °C, the value of T_{d5} increased significantly to 340 °C and the char yield was approximately 55 wt%. This char yield is higher than that of conventional 3-phenyl-3,4-dihydro-2*H*-benzoxazine (*ca.* 48 wt%) at 700 °C, indicating a more highly cross-linked structure arising from the presence of the azine groups, as well as from intramolecular hydrogen bonding involving the azine groups [Scheme 1(d)]. Fig. 7 presents the PL spectra of pure azine-BZ obtained after thermal curing at various temperatures. The maximum

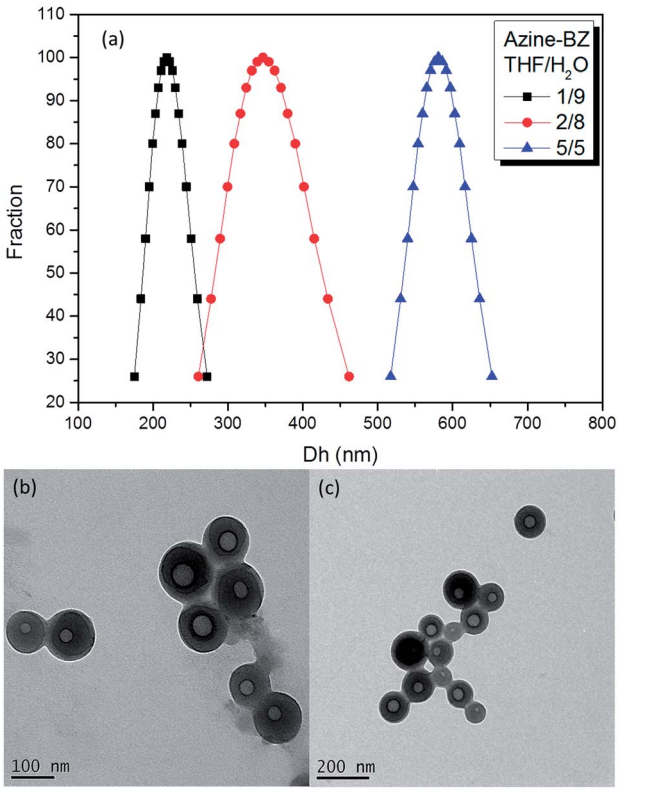

Fig. 4 (a) Particle size distributions of azine-BZ in THF/water mixtures at water fractions of 50%, 80%, and 90%. TEM images of azine-BZ at a concentration of 1.0×10^{-4} mol L^{-1} in THF/water mixtures at ratios of (b) 20 : 80 and (c) 10 : 90 (v/v).

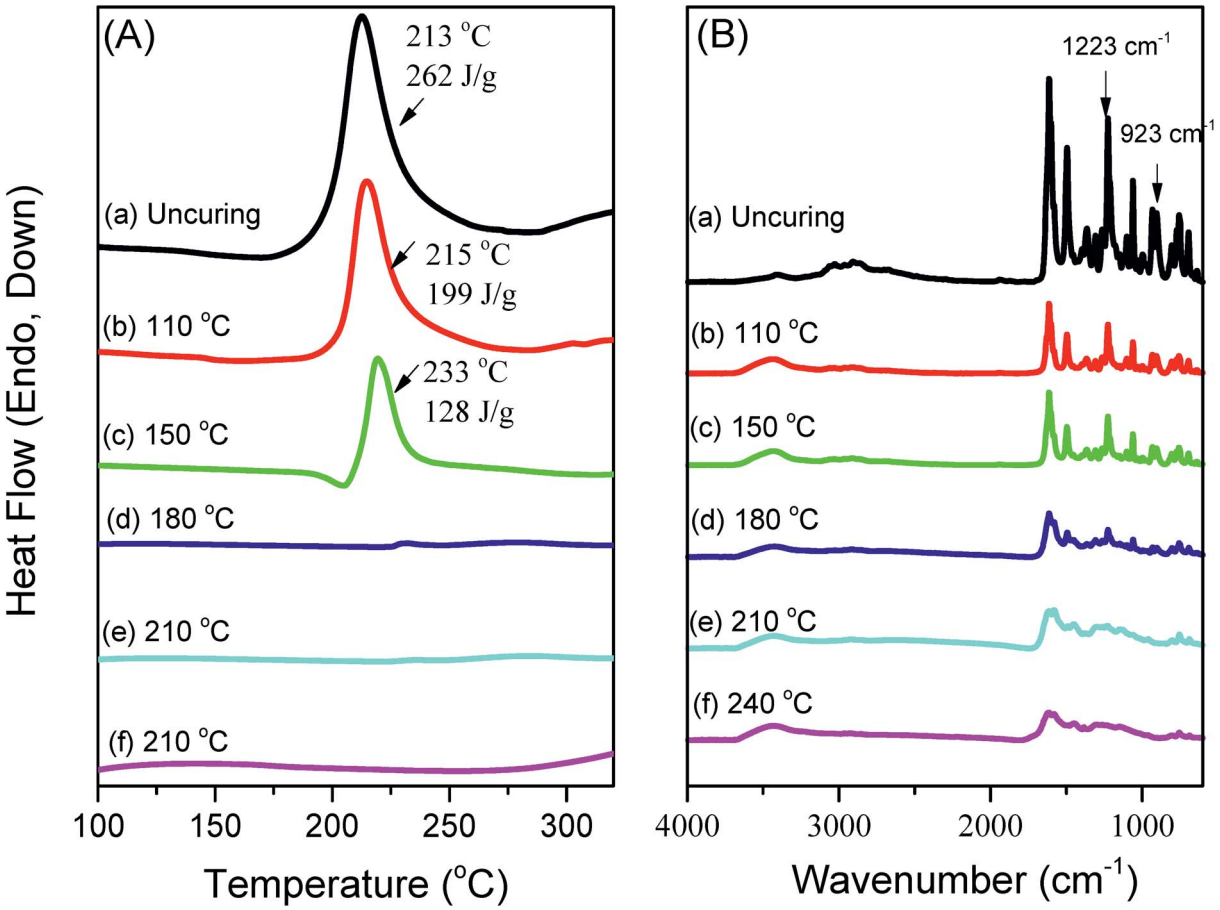

Fig. 5 (A) DSC profile and (B) FTIR spectra of azine-BZ monomer recorded after thermal treatments.

intensity emission of the uncured azine-BZ was higher than those after curing. Interestingly, azine-BZ still emitted light after curing at 150 °C. The ^{1}H NMR spectrum of azine-BZ after thermal curing at 150 °C indicated that ring-opening polymerization had not occurred: the two peaks at 4.70 and 5.33 ppm representing the oxazine ring were still present [Fig. S5(b)†]. The emission was quenched after curing at 180, 210, and 240 °C. As a result, the emission from azine could also be used as a probe of the extent of curing of the BZ monomer. Fig. 8 summarizes the PL intensity of pure azine-BZ after each curing and DSC thermal scan. The emission intensity was quenched after curing at 180 °C [Fig. 8(b)], which is consistent with the initial thermal curing based on DSC analysis [Fig. 8(a)]. In addition, the characteristic absorption bands at 923 cm^{-1} disappeared completely after curing at 180 °C [Fig. 5(B)]. To the best of our knowledge, this report provides the first example of emission behavior being used to monitor curing behavior in a manner consistent with DSC and FTIR spectroscopic data.

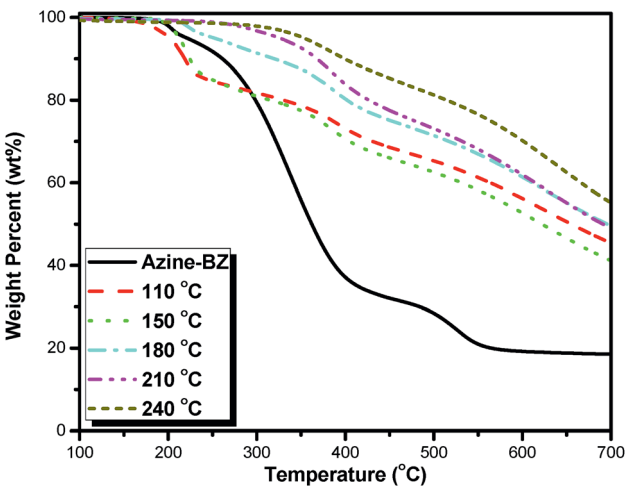

Fig. 6 Thermogravimetric analyses of azine-BZ monomer, recorded after thermal polymerization at 110, 150, 180, 210 and 240 °C.

AIE phenomena and thermal polymerization of azine-BZ/$Zn(ClO_4)_2$ complexes

The thermal uncuring behavior of azine-BZ/$Zn(ClO_4)_2$ complexes was investigated using DSC and FTIR. Fig. 9 reveals that the thermal curing peaks shifted to lower temperature upon increasing the $Zn(ClO_4)_2$ content, decreasing from 213 °C to 184 °C in the presence of 10 wt% $Zn(ClO_4)_2$, suggesting that the Zn^{2+} ions enhanced the ring opening process.[39–41] FTIR analyses were carried out to investigate the specific interaction (metal–ligand interaction) of azine-BZ after it was blended with

various $Zn(ClO_4)_2$ contents at ambient temperature and the spectra are displayed in Fig. 10. Analysis of these spectra suggests that the shifts observed in the absorption peaks of the polymer structures were caused by specific ion–dipole interactions. Concentrating on the azine band at 1632 cm^{-1}, we assign the new band at 1664 cm^{-1} that appeared at 5 or 10 wt% $Zn(ClO_4)_2$ to the azine groups coordinating as π-bonding ligands to zinc cations (inset to Fig. 10). Therefore, the higher energy of this new absorption was due to the formation of such a metal–ligand complex.

In addition, the thermal polymerization of azine-BZ/5 wt% $Zn(ClO_4)_2$ complex was studied by DSC measurement. As revealed in Fig. 11(A), the enthalpy of the curing exotherm decreased gradually upon increasing the temperature of the curing process, reaching zero at a curing temperature of 180 °C. Fig. 11(B) presents the corresponding FTIR spectra obtained after thermal curing of the 5 wt% $Zn(ClO_4)_2$ blend at various temperatures. The characteristic absorption bands of the oxazine units at 1223 and 931 cm^{-1} disappeared after thermal curing at temperatures from 180 to 240 °C. Much literature reported that there are numerous catalysts (*e.g.* Li^+, Fe^{3+}…) that can act as effective promoters and accelerators for the ring-opening polymerization of benzoxazine. The mechanism of ring-opening polymerization of benzoxazines using catalyst is divided into three steps: coordination-ring opening, electrophilic attack and finally rearrangement leading to phenolic and phenoxy structure.[42] We suspect that the Zn^{2+} ions coordinated effectively to the O and/or N atoms during ring opening of the BZ units; Scheme 2 presents some possible structures.

As mentioned above, the salicylaldehyde azine derivatives exhibit AIE features and emit light in their aggregated state because of the restricted rotation of their N–N single bonds; in addition, salicylaldehyde azines bearing *ortho* OH groups on their phenyl rings can undergo intramolecular hydrogen bonding, which could lead to excited state intramolecular proton transfer (ESIPT).[33,43] Azine-BZ exhibits weak emission

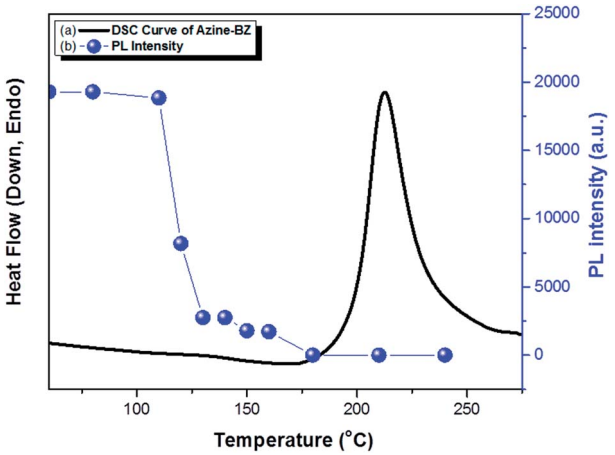

Fig. 8 (a) DSC scan and (b) PL intensity of pure azine-BZ monomer after each thermal curing stag.

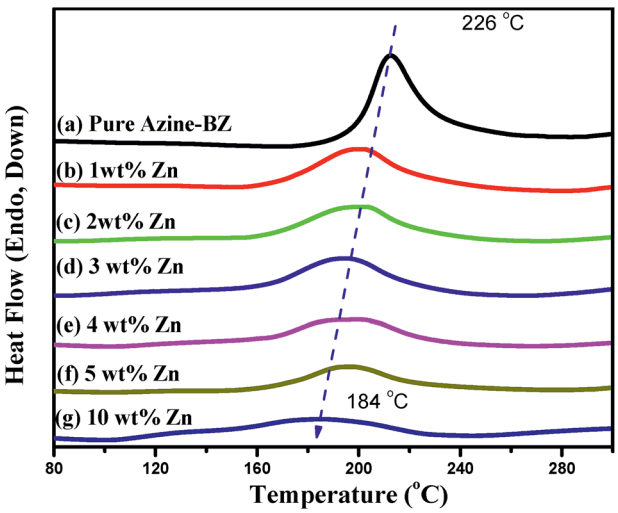

Fig. 9 DSC thermograms of azine-BZ in the presence of various weight ratios of $Zn(ClO_4)$.

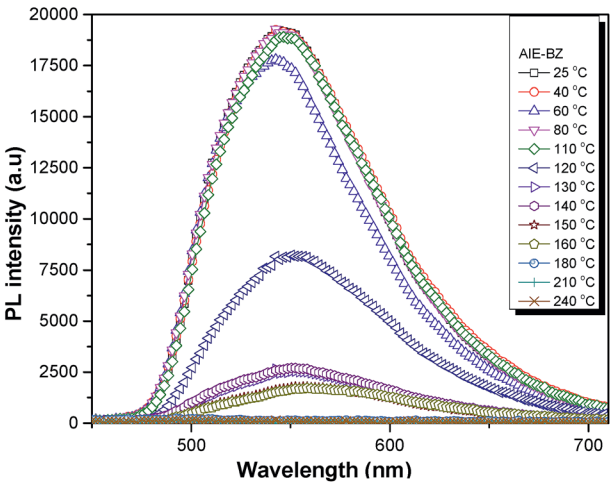

Fig. 7 PL spectra of azine-BZ monomer in the bulk state, recorded after each curing stage.

in solution because of intramolecular hydrogen bonding between the phenolic OH group and the N atom of the imino group that undergoes ESIPT phenomena. We were also interested in examining the AIE-active behavior of azine-BZ when blended with $Zn(ClO_4)_2$. Fig. 12 presents the PL spectra of azine-BZ in the presence of various amounts of $Zn(ClO_4)_2$ in the bulk state. Interestingly, the PL intensities when the contents of zinc ions were 1, 2, 3, and 4 wt% were higher than that of pure azine-BZ due to the Zn^{2+} ion having closed-shell d-orbitals; thus, the energy transfer process could not occur, leading to enhanced metal–ligand charge transfer (MLCT),[36,37] as depicted in Scheme 2. In contrast, the PL intensity decreased when the content of Zn^{2+} ions was 5 or 10 wt%, presumably because the Zn^{2+} ions coordinated to the azine units, as displayed in Fig. 10, changing the mechanism of the MLCT. To further study the optical properties of the aggregated azine-BZ/3 wt% Zn^{2+} ion complex, we examined

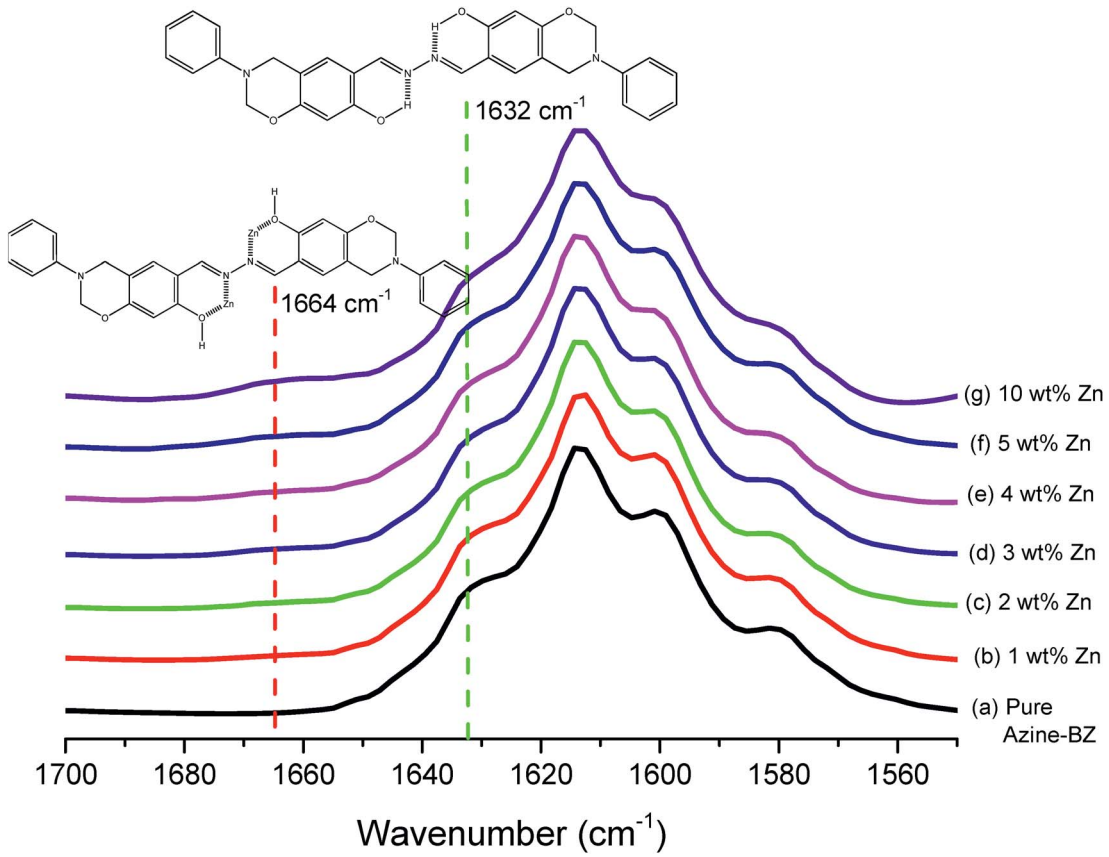

Fig. 10 FTIR spectra of azine-BZ in the presence of various amounts of $Zn(ClO_4)_2$ recorded at ambient temperature.

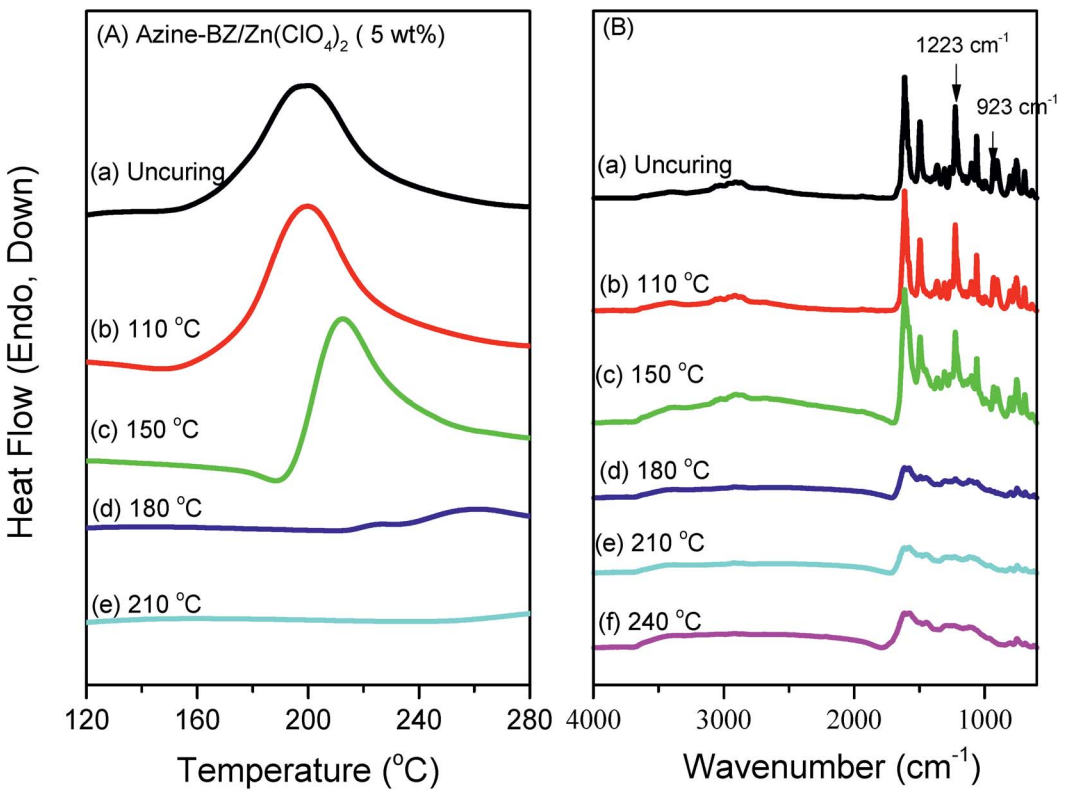

Fig. 11 (A) DSC thermograms and (B) FTIR spectra of azine-BZ monomer in the presence of 5 wt% $Zn(ClO_4)_2$ recorded after each curing stage.

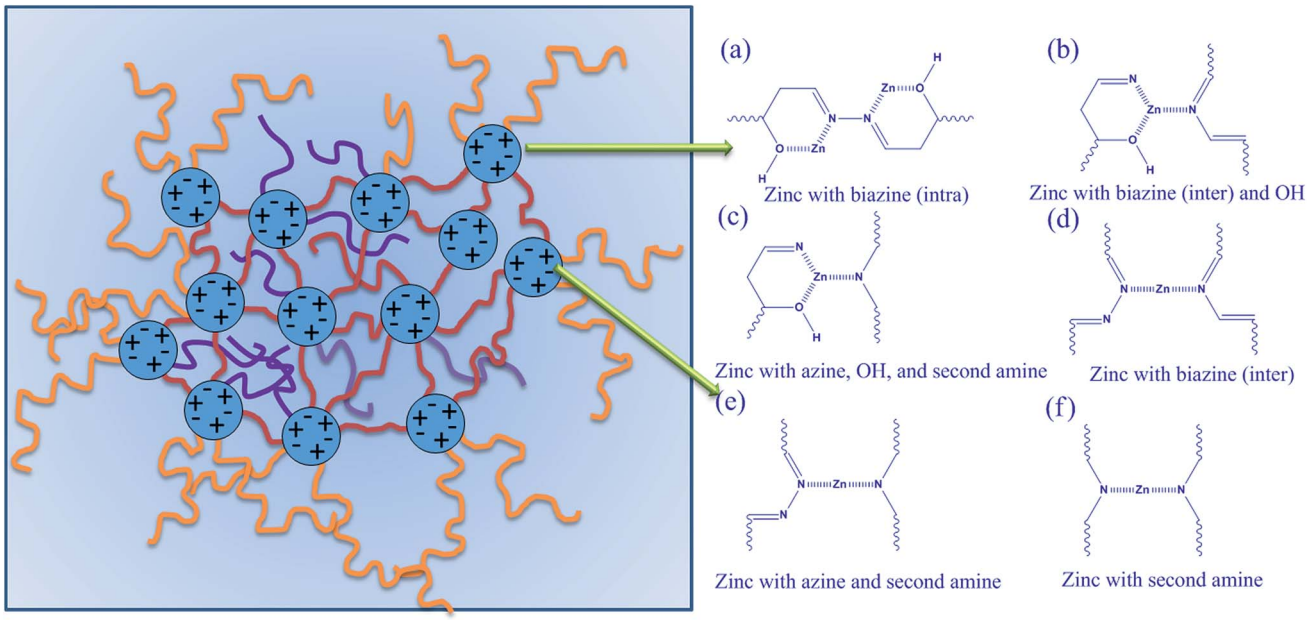

Scheme 2 (Left) Possible model of a poly(azine-BZ)/$Zn(ClO_4)_2$ complex. (Right) Possible modes of metal–ligand complexes between $Zn(ClO_4)_2$ and poly(azine-BZ).

fluorescence in THF in the presence of a poor solvent (water). As revealed in Fig. 13, azine-BZ in the presence of 3 wt% Zn^{2+} ions in pure THF displayed a non-emissive PL intensity, with the PL intensity increasing upon the addition of water up to a fraction of 90%—characteristic AIE behavior. Fig. 14 presents the PL spectra of azine-BZ/3 wt% $Zn(ClO_4)_2$ complex after thermal curing at various temperatures. The PL intensity of this complex was higher than that of pure azine-BZ prior to curing, consistent with MLCT. Upon increasing the curing temperature, the PL intensity decreased gradually until the quenching was completed at curing temperatures from 180 to 240 °C, similar to the behavior of the pure azine-BZ monomer.

Fig. 15 presents the thermal stability of azine-BZ blended with various contents of $Zn(ClO_4)_2$ after thermal curing at 210 °C under N_2 at heating rate 20 °C min^{-1}, as investigated using TGA. As expected, the thermal decomposition temperature and char yield both increased upon increasing the $Zn(ClO_4)_2$ content. We found that the decomposition temperature value (T_{d5}) and char yield for the azine-BZ/5 wt% Zn^{2+} complex was higher (350 °C, 61 wt%) than that for pure azine-BZ (312 °C, 48 wt%), because the Zn^{2+} ions increased the degree of cross-linking (inset to Fig. 15), in addition to the crosslinking

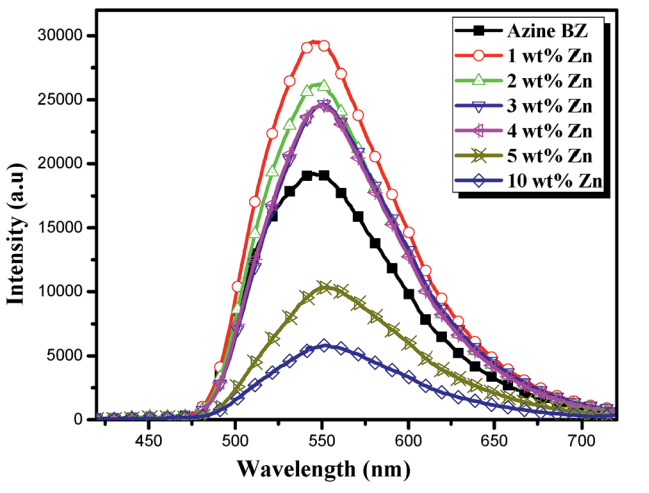

Fig. 12 PL spectra of azine-BZ blended with various weight ratios of $Zn(ClO_4)_2$ in the bulk state, recorded at room temperature.

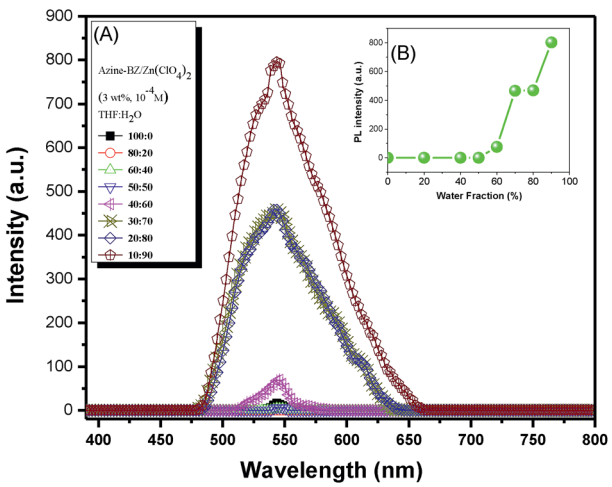

Fig. 13 (A) PL spectral changes and (B) PL intensities of azine-BZ blended with 3 wt% $Zn(ClO_4)_2$ (1.0×10^{-4} mol L^{-1}) in THF/water mixtures at various water fractions.

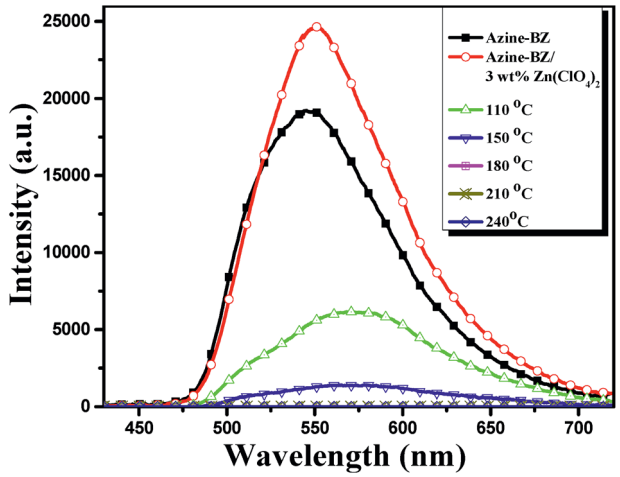

Fig. 14 PL spectra of azine-BZ blended with 3 wt% $Zn(ClO_4)_2$ in the bulk state, recorded at room temperature after each thermal curing stage.

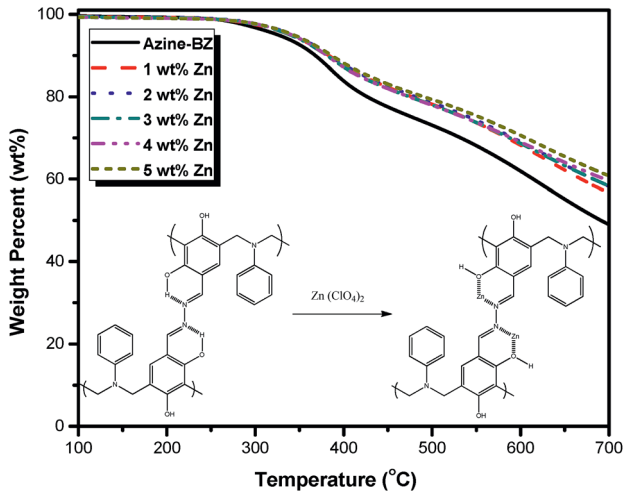

Fig. 15 TGA analyses of azine-BZ blended with various amounts of $Zn(ClO_4)_2$, recorded after thermal curing at 210 °C.

through intra- and inter-molecular hydrogen bonding after ring opening.

Conclusions

A new azine-based BZ monomer has been designed that exhibits aggregation induced emission (AIE) behavior. DSC analysis revealed that the exothermic peak for the ring opening polymerization of azine-BZ shifted to lower temperature, compare to that for a standard BZ, because the basicity of the phenolic unit facilitated the ring opening process. Furthermore, the azine unit in the BZ monomer has high affinity for Zn^{2+} ions, promoting ring opening polymerization at a lower curing temperature (from 213 °C in the absence of the Zn^{2+} ions to 184 °C in their presence). Based on thermogravimetric results, the improvement of thermal stability of azine-BZ/$Zn(ClO_4)_2$ complexes is due to the presence of strong polymer–metal complexes. Azine-BZ coordinated with $[Zn(ClO_4)_2]$ through metal–ligand interactions, increasing the fluorescence emission intensity relative to that of the pure azine-BZ monomer, is a result of MLCT. The PL properties of the azine units and the metal–ligand complexes suggest that such monomers might act as probes for realizing the thermal curing behavior of BZ rings; as fluorescent chemosensors for Zn^{2+} and other transition metal ions, even at high curing temperatures (*e.g.*, 150 °C); and as components within polymer/inorganic hybrid materials.

Acknowledgements

This study was supported financially by the Ministry of Science and Technology, Taiwan, Republic of China, under contracts MOST103-2221-E-110-079-MY3 and MOST102-2221-E-110-008-MY3. We thank Mr Hsien-Tsan Lin of the Regional Instruments Center at National Sun Yat-Sen University for help with the TEM experiments.

References

1 H. Ishida, *Handbook of Polybenzoxazine*, ed. H. Ishida and T. Agag, Elsevier, Amsterdam, 2011, ch. 1, p. 1.
2 N. Ghosh, B. Kiskan and Y. Yagci, *Prog. Polym. Sci.*, 2007, **32**, 1344–1391.
3 Y. Yagci, B. Kiskan and N. N. Ghosh, *J. Polym. Sci., Part A: Polym. Chem.*, 2009, **47**, 5565–5576.
4 (*a*) T. Takeichi and T. Agag, *High Perform. Polym.*, 2006, **18**, 777–797; (*b*) Y. X. Wang and H. Ishida, *Polymer*, 1999, **40**, 4563–4570; (*c*) M. Zhang, Z. Tan, S. Hu, J. Qiu and C. Liu, *RSC Adv.*, 2104, **4**, 44234–44243.
5 (*a*) H. Ishida and Y. H. Lee, *Polym. Polym. Compos.*, 2011, **9**, 121–134; (*b*) H. D. Kim and H. Ishida, *J. Phys. Chem. A*, 2002, **106**, 3271–3280; (*c*) H. D. Kim and H. Ishida, *Macromol. Symp.*, 2003, **195**, 123–140; (*d*) S. W. Kuo, Y. C. Wu, C. F. Wang and K. U. Jeong, *J. Phys. Chem. C*, 2009, **13**, 20666–20673; (*e*) C. F. Wang, S. F. Chiou, F. H. Ko, J. K. Chen, C. T. Chou, C. F. Huang, S. W. Kuo and F. C. Chang, *Langmuir*, 2007, **23**, 5868–5871; (*f*) W. H. Hu, K. W. Huang and S. W. Kuo, *Polym. Chem.*, 2012, **3**, 1546–1554.
6 (*a*) Q. Li and X. Zhong, *Langmuir*, 2007, **27**, 8365–8369; (*b*) H. Oie, A. Sudo and T. Endo, *J. Polym. Sci., Part A: Polym. Chem.*, 2011, **49**, 3174–3183; (*c*) A. Sudo, R. Kudo, H. Nakuyama, K. Airma and T. Endo, *Macromolecules*, 2008, **41**, 9030–9034; (*d*) S. W. Kuo and F. C. Chang, *Prog. Polym. Sci.*, 2011, **36**, 1649–1696; (*e*) M. G. Mohamed, K. C. Hsu and S. W. Kuo, *Polym. Chem.*, 2015, **6**, 2423–2433; (*f*) C. Li, Q. Ran, R. Zhu and Y. Gu, *RSC Adv.*, 2015, **5**, 22593–22600.
7 C. K. Chozhan, M. Alagar and P. Gnanasundarm, *Acta Mater.*, 2009, **28**, 338–794.
8 M. G. Mohamed, H. K. Shih and S. W. Kuo, *RSC Adv.*, 2015, **5**, 12763–12772.
9 H. Ishida and H. Y. Low, *Macromolecules*, 1997, **30**, 1099–1106.

10 T. Agag and T. Takeichi, *Polymer*, 2000, **41**, 7083–7090.
11 P. Phirivawirut, R. Magaraphan and H. Ishida, *Mater. Res. Innovations*, 2001, **4**, 187–198.
12 M. R. Vengatesan, S. Devaraiu, K. Dinkaran and M. Alagar, *J. Mater. Chem.*, 2012, **22**, 7559.
13 C. F. Wang, Y. C. Su, S. W. Kuo, C. F. Huang, Y. C. Sheen and F. C. Chang, *Angew. Chem., Int. Ed.*, 2006, **45**, 2248–2251.
14 T. Agag, R. C. Arza, F. H. J. Maurer and H. Ishida, *Macromolecules*, 2010, **43**, 2748–2758.
15 A. Chernykh, T. Agag and H. Ishida, *Polymer*, 2009, **50**, 3153–3157.
16 H. M. Qi, G. Y. Pan and Q. Y. Zhuang, *Polym. Eng. Sci.*, 2010, **50**, 1751–1757.
17 Z. Brunovska and H. Ishida, *J. Appl. Polym. Sci.*, 1999, **73**, 2937–2949.
18 T. Takeichi, K. Nakamura, T. Agag and H. Muto, *Des. Monomers Polym.*, 2004, **7**, 727–740.
19 R. Kudoh, A. Sudo and T. Endo, *Macromolecules*, 2010, **43**, 1185–1187.
20 Y. C. Ye, Y. J. Huang, F. C. Chang, Z. G. Xue and X. L. Xie, *Polym. Chem.*, 2014, **5**, 2863–2871.
21 (*a*) J. Liu, C. Scott, S. Winroth, J. Maia and H. Ishida, *RSC Adv.*, 2015, **5**, 16785–16791; (*b*) K. Sethuraman and M. Alagar, *RSC Adv.*, 2015, **5**, 9607–9617; (*c*) R. Sasikumar, M. Ariraman and M. Alagar, *RSC Adv.*, 2014, **4**, 19127–19136.
22 S. W. Thomass, G. D. Joly and T. M. Swager, *Chem. Rev.*, 2007, **107**, 1339–1386.
23 C. T. Chen, *Chem. Mater.*, 2004, **16**, 4389–4400.
24 R. T. K. Kwok, J. L. Geong, J. W. Y. Lam, E. G. Zhao, G. Wang, R. Y. Zhan, B. Liu and B. Z. Tang, *J. Mater. Chem. B*, 2014, **2**, 4134.
25 Y. Q. Dong, J. W. Y. Lam, A. J. Qin, Z. Li, J. Z. Sun, H. Y. Sung, I. D. Williams and B. Z. Tang, *Chem. Commun.*, 2007, 40–42.
26 H. Saigusa and E. C. Lim, *J. Phys. Chem.*, 1995, **99**, 15738–15747.
27 J. Luo, Z. Xie, J. W. Y. Lam, L. Cheng, H. Chen, C. Qiu, H. S. Kwok, X. Zhan, Y. Liu, D. Zhu and B. Z. Tang, *Chem. Commun.*, 2001, 1740–1741.
28 J. Chen, C. C. W. Law, J. W. Y. Lam, Y. Dong, S. M. F. Lo, I. D. Williams, D. Zhu and B. Z. Tang, *Chem. Mater.*, 2003, **15**, 1535–1546.
29 Y. P. Li, F. Li, H. Y. Zhang, Z. Q. Xie, W. J. Xie, H. Xu, B. Li, F. Y. Z. Shen and L. M. Hanif, *Chem. Commun.*, 2007, 231–233.
30 Z. P. Yu, Y. Y. Duan, L. H. Cheng, Z. L. Han, Z. Zheng, H. P. Zhou, J. Y. Wu and Y. P. Tian, *J. Mater. Chem.*, 2012, **22**, 16927–16932.
31 Y. Qian, M. M. Cai, X. H. Zhou, Z. Q. Gao, X. P. Wang, Y. Z. Zhao, X. H. Yan, W. Wei, L. H. Xie and W. Huang, *J. Phys. Chem. C*, 2012, **116**, 12187–12195.
32 Z. Q. Xie, B. Yang, G. Cheng, L. L. Liu, F. He, F. Z. Shen, Y. G. Ma and S. Y. Liu, *Chem. Mater.*, 2005, **17**, 1287–1289.
33 W. Tang, Y. Xiang and A. Tong, *J. Org. Chem.*, 2009, **74**, 2163–2166.
34 S. L. Liu, D. Li, Z. Zhang, G. K. S. Prakash, P. S. Conti and Z. B. Li, *Chem. Commun.*, 2014, **50**, 7371.
35 L. L. Long, W. Y. Lin, B. B. Chen, W. S. Gao and L. Yuan, *Chem. Commun.*, 2011, **47**, 893.
36 B. K. An, S. K. Kwon, S. D. Jung and S. Y. Park, *J. Am. Chem. Soc.*, 2002, **124**, 14410–14415.
37 W. Tang, Y. Xiang and A. Tong, *J. Org. Chem.*, 2009, **74**, 2163–2166.
38 G. Liu, M. Yang, L. Wang, J. Zheng, H. Zhou, J. Wu and Y. Tian, *J. Mater. Chem. C*, 2014, **2**, 2684–2691.
39 M. G. Mohamed, W. C. Su, Y. C. Lin, C. F. Wang, J. K. Chen, K. U. Jeong and S. W. Kuo, *RSC Adv.*, 2014, **4**, 50373–50385.
40 Y. H. Low and H. Ishida, *Polym. Degrad. Stab.*, 2006, **91**, 805–815.
41 O. T. Lekesiz and J. Hacaloglu, *Polymer*, 2014, **55**, 3533–3542.
42 C. Liu, D. Shen, M. R. Sebastian, J. Marquet and R. Schonfold, *Macromolecules*, 2011, **44**, 4616–4622.
43 T. S. Hsiao, S. L. Deng, K. Y. Shih and J. L. Hong, *J. Mater. Chem. C*, 2014, **2**, 4828–4834.